Model-Based Online Detection, Quantification and Localization of Internal Short Circuits in Lithium-Ion Pouch Cells via an Unscented Kalman Filter

Lorenzo Brancato[1], Yiqi Jia[2], Danyang Wang[3], Marco Giglio[4]and Francesco Cadini[5]

[1,2,3,4,5] *Politecnico di Milano, Milan, Italy*
lorenzo.brancato@polimi.it
yiqi.jia@polimi.it
danyang.wang@polimi.it
marco.giglio@polimi.it
francesco.cadini@polimi.it

ABSTRACT

Internal short circuits (ISCs) are a leading precursor of thermal runaway in lithium-ion batteries, yet they are difficult to observe directly because their early electrical signature is small and ambiguous and their thermal signature is spatially distributed. This paper presents a model-based observer that simultaneously detects an ISC, quantifies its severity, and localizes it on the surface of a pouch cell using only the applied current, the terminal voltage, and a small array of surface temperature sensors. A lumped electro-thermal model couples a third-order equivalent-circuit model (ECM) of the cell to a two-dimensional lumped-parameter thermal network (LPTN); the ISC is parameterized by a shunt conductance G and a planar location (x, y), and is the source of an additional ohmic heat term injected locally into the thermal field. These three fault parameters are appended to the dynamic state and estimated online with a single joint unscented Kalman filter (UKF). A location-observability gate suppresses spurious position updates until the measured spatial thermal contrast is informative, and the detection instant is defined as the time at which the filter covariance converges to a stable value. The method is evaluated on a design of experiments (DoE) of sub-critical shorts generated by a high-fidelity electrochemical–thermal plant, spanning three severities and nine locations. For strong and moderate shorts the observer recovers severity to within about 7% and location to within about 2 mm, converging in roughly 110 s; for the weakest short the severity is quantifiable only to order of magnitude and the thermal contrast is insufficient to localize, defining the detectability floor of the sensing arrangement.

1. INTRODUCTION

Lithium-ion cells underpin electrified transport and grid storage, and their safe operation depends on detecting incipient faults before they escalate. Among these faults, the internal short circuit (ISC) is particularly hazardous: a local breakdown of the separator creates a conductive bridge between electrodes that dissipates energy as heat and, if unchecked, can drive the cell into thermal runaway (Feng et al., 2018; Wang et al., 2012). The early window is the actionable one: a nascent short releases comparatively little power and does not immediately threaten the pack, yet it is precisely in this sub-critical phase that intervention is still possible.

Diagnosing the short this early is difficult not because it leaves no trace at all, but because the traces it leaves are ambiguous. The parasitic current drawn by the fault is initially a small fraction of the operating current, so the deviation it produces on the terminal voltage, while measurable, is of the same order as the prediction error of any reduced cell model and carries no information whatsoever about *where* the fault sits. The heat released by the short does carry that information, but it is deposited locally and is only weakly observed by a sparse set of surface sensors. Severity and position are therefore reached through two different channels with very different signal-to-noise characteristics, which is the central difficulty addressed in this work.

The ISC itself is a heterogeneous phenomenon. It can arise from manufacturing contaminants, lithium plating and dendrite growth, mechanical deformation, or separator aging, and the resulting metallic bridge may take very different resistances depending on the contacting materials (Santhanagopalan, Ramadass, & Zhang, 2009; Huang et al., 2021). This variability, together with the impossibility of prescribing a known short in a healthy commercial cell without destroying it, makes experimental ground truth scarce and motivates the use of validated electrochemical–thermal simulation to generate labeled fault scenarios with known severity and location (Feng et al., 2015).

Methods for ISC diagnosis fall into two broad families. Data-driven approaches learn fault signatures from voltage, current and temperature features, or detect abnormal cell-to-cell consistency within a pack (Seo, Goh, Park, Koo, & Kim, 2017; Kang, Duan, Zhou, Shang, & Zhang, 2019); they are effective when representative labeled data are available, but they generalize poorly to unseen geometries, severities and operating conditions, and they seldom yield a physical fault location. Model-based approaches instead embed a physical description of the cell in an observer and estimate fault parameters as part of the state. They are interpretable, degrade gracefully, and naturally produce severity and, in principle, location (Schwabacher & Goebel, 2007). The terminal behavior of the cell is most commonly captured by an equivalent-circuit model (ECM), whose order and parameterization trade fidelity against computational cost (Hu, Li, & Peng, 2012), while reduced electrochemical models such as the Doyle–Fuller–Newman (DFN) formulation (Doyle, Fuller, & Newman, 1993) provide higher fidelity at higher cost and are increasingly accessible through open simulation frameworks (Sulzer, Marquis, Timms, Robinson, & Chapman, 2021).

Both families have moved well beyond their classical forms in recent years, and the choice made here should be read against those alternatives. On the data-driven side, deep networks trained on large cycling datasets extract degradation and fault signatures that hand-crafted features miss (Severson et al., 2019), and physics-informed formulations embed the governing balances directly in the learner, so that far less labeled data is required and the output remains physically consistent (Nascimento, Corbetta, Kulkarni, & Viana, 2021). On the model-based side, particle filters relax the Gaussian assumption of the Kalman family at the price of a sample budget one to two orders of magnitude larger (Miao, Xie, Cui, Liang, & Pecht, 2013); moving-horizon estimation replaces the recursive update with a constrained optimization over a trailing window, which handles bounds on the fault parameters rigorously but requires solving a nonlinear program at every step (Rao, Rawlings, & Mayne, 2003); adaptive observers track parameters at very low cost but return no measure of uncertainty (Besançon, 2000); and joint electrochemical estimation propagates the state of a reduced physics model instead of a circuit, buying fidelity with a substantially heavier online model (Bizeray, Zhao, Duncan, & Howey, 2015). Judged against the requirement addressed here — an online estimate of severity *and* position, accompanied by a calibrated confidence, on a computational budget compatible with a battery management system — the sigma-point filters remain the natural choice: they are derivative-free, cost a fixed multiple of one model evaluation per sample, and maintain the covariance on which the detection criterion of this paper is built, whereas the data-driven family returns no fault position and the optimization-based estimators return one only at a cost that is difficult to sustain online.

Observing an ISC also requires representing where its heat goes. Cell heat generation is classically described by the reversible and irreversible terms of the Bernardi energy balance (Bernardi, Pawlikowski, & Newman, 1985), and the resulting temperature field is well captured for online use by lumped-parameter thermal networks (Forgez, Do, Friedrich, Morcrette, & Delacourt, 2010). Because a short is a *localized* source, the spatial temperature distribution carries information about its position; resolving that position, however, requires both a spatially resolved thermal model and sensors arranged to see the contrast it produces. Most existing model-based work detects and quantifies an ISC but stops short of localizing it, and the few schemes that address location typically do so offline or with dense instrumentation.

This paper develops a single joint UKF that detects, quantifies *and* localizes an ISC online from current, voltage and five surface temperatures. The contributions are: (i) a compact coupled ECM–LPTN observer model in which the ISC is represented by a conductance and a planar position acting as a localized heat source; (ii) a joint estimation scheme, with a location-observability gate and a covariance-convergence detection criterion, that exploits the cross-coupling between severity and the thermal field; and (iii) an evaluation on a design of experiments (DoE) of sub-critical shorts produced by a high-fidelity electrochemical–thermal plant, which characterizes the achievable quantification and localization accuracy and the detectability floor of the sensor layout.

Throughout, the fault severity is parameterized in the model by the shunt conductance G, which is the quantity actually appended to the state and estimated, and is *reported* as the equivalent short resistance $R_{\mathrm{ISC}} = 1/G$, which is the form used in the ISC literature; the two are used interchangeably in this sense and never denote different quantities.

2. SYNTHETIC PLANT AND DESIGN OF EXPERIMENTS

To obtain ground-truth severities and locations that are not available from physical testing, the observer is evaluated against a high-fidelity *plant* model that is deliberately more detailed than the observer's internal model. The plant couples a pseudo-two-dimensional Doyle–Fuller–Newman (DFN) electrochemical model of the cell (Doyle et al., 1993) to a three-dimensional thermal model of the pouch, solved on a fine mesh. The two physics are two-way coupled, as sketched in Figure 1: the electrochemical model supplies the reversible and irreversible heat generation that drives the thermal field, while the averaged cell temperature feeds back into the temperature-dependent transport and kinetic parameters of the electrochemical model. The ISC is superimposed as a shunt path of conductance G at a prescribed in-plane location; it draws a parasitic current proportional to the local cell voltage and deposits the corresponding ohmic power as a localized heat source in the thermal mesh. All cases studied here are *sub-critical*: the injected power is small enough that thermal runaway is not triggered, so the scenarios represent the early, actionable window for diagnosis.

Because the plant and the observer differ in structure — a distributed electrochemical description against a lumped circuit, a three-dimensional mesh against a two-dimensional network — the evaluation is not a self-consistency check of a single model against itself, and the residual biases reported in Section 5.3 are genuine model-mismatch effects rather than numerical artifacts.

The design of experiments spans three short severities, $R_{\mathrm{ISC}} \in \{1, 10, 100\}\ \Omega$ (i.e. $G \in \{1, 0.1, 0.01\}$ S), at nine in-plane locations arranged on a regular 3×3 grid over the cell face, giving 27 scenarios. Each scenario is a 1C discharge from an initial state of charge of 0.99 into a 25°C environment ($h = 35\ \mathrm{W\,m^{-2}K^{-1}}$), sampled every $\Delta t = 5$ s, with zero-mean Gaussian noise of standard deviation 10 mV added to the terminal voltage and 0.1 K to each of the five surface temperature sensors. The cell geometry, the location grid and the sensor layout are shown in Figure 2. The sensors follow a quincunx pattern (one central, four near the corners), which is the smallest arrangement able to resolve in-plane position by thermal contrast. All 27 cases share a single operating condition — one discharge profile, one ambient temperature and one sampling rate — so the DoE characterizes performance across fault realizations rather than robustness across duty cycles; this restriction is revisited in Section 5.3.

3. OBSERVER MODEL

The observer uses a reduced electro-thermal model that is fast enough to run inside the filter while retaining the physics needed to make the fault parameters observable.

3.1. Electrical Model

The cell terminal behavior is described by a third-order Thévenin equivalent-circuit model (ECM). The state comprises the state of charge z and three relaxation voltages $V_{\mathrm{RC},i}$, $i = 1, 2, 3$. The open-circuit voltage $\mathrm{OCV}(z, T)$, the series resistance $R_0(z, T)$ and the three R_i–τ_i pairs are stored as look-up tables identified offline and interpolated at the running z and mean cell temperature T. The ISC is modeled as a conductance G in parallel with the terminals. With applied current u, the terminal voltage and the total current through the cell follow from the parallel combination,

$$V_t = \frac{\mathrm{OCV}(z,T) - \sum_i V_{\mathrm{RC},i} - R_0\, u}{1 + R_0\, G}, \tag{1}$$

and $I_{\mathrm{tot}} = u + V_t\, G$, where $V_t\, G$ is the parasitic short current. The state of charge integrates I_{tot} through the cell capacity and the relaxation voltages follow the usual first-order dynamics with time constants τ_i.

3.2. Thermal Model

The in-plane temperature distribution is represented by a two-dimensional lumped-parameter thermal network (LPTN): the cell face is discretized into an $N = N_x \times N_y$ grid of nodes with in-plane conduction between neighbors and convective exchange with the environment from the faces and edges. Collecting the nodal temperatures in a vector $\mathbf{T}$, the network obeys the linear state equation

$$\dot{\mathbf{T}} = \mathbf{A}_{\mathrm{th}}\, \mathbf{T} + \mathbf{B}_{\mathrm{th}}\, T_{\mathrm{env}} + \mathbf{C}^{-1}\mathbf{Q}, \tag{2}$$

where $\mathbf{A}_{\mathrm{th}}$ and $\mathbf{B}_{\mathrm{th}}$ derive from the conductance and capacitance matrices and $\mathbf{Q}$ is the nodal heat input. Over one sampling interval Δt with constant forcing, Eq. (2) is advanced by the exact discrete map $\mathbf{T}_{k+1} = \mathbf{A}_d \mathbf{T}_k + \mathbf{M}_d \mathbf{f}_k$, with $\mathbf{A}_d = e^{\mathbf{A}_{\mathrm{th}}\Delta t}$ and $\mathbf{M}_d = \mathbf{A}_{\mathrm{th}}^{-1}(\mathbf{A}_d - \mathbf{I})$.

The heat input has two parts. A spatially uniform contribution accounts for the reversible (entropic) and irreversible cell heat, $Q_{\mathrm{cell}} = I_{\mathrm{tot}}(\mathrm{OCV} - V_t) + I_{\mathrm{tot}}\, T\, \partial U/\partial T$. The short contributes an additional ohmic power $Q_{\mathrm{ISC}} = V_t^2\, G$ deposited around the fault location (x, y) through a normalized Gaussian kernel of fixed spread, so that the location enters the model only through where this heat is injected,

$$\mathbf{Q} = \frac{Q_{\mathrm{cell}}}{N}\mathbf{1} + Q_{\mathrm{ISC}}\, \mathbf{w}(x, y), \quad w_j \propto e^{-\|\mathbf{r}_j - (x,y)\|^2/2\sigma_k^2}. \tag{3}$$

The measurement model returns the terminal voltage from Eq. (1) and the temperatures at the sensor nodes.

4. JOINT ESTIMATION

4.1. Augmented State and Filter

Detection, quantification and localization are posed as a single joint state-estimation problem. The dynamic state of the electrical and thermal models is augmented with the three fault parameters,

$$\mathbf{x} = \left[\, z,\ V_{\mathrm{RC},1:3},\ \mathbf{T},\ G,\ x,\ y \,\right]^{\top}, \tag{4}$$

which are treated as slowly varying (random-walk) quantities with a small process noise. The augmented system is propagated by an unscented Kalman filter, which represents the state distribution by a deterministic set of sigma points passed through the nonlinear model, avoiding linearization (Julier &

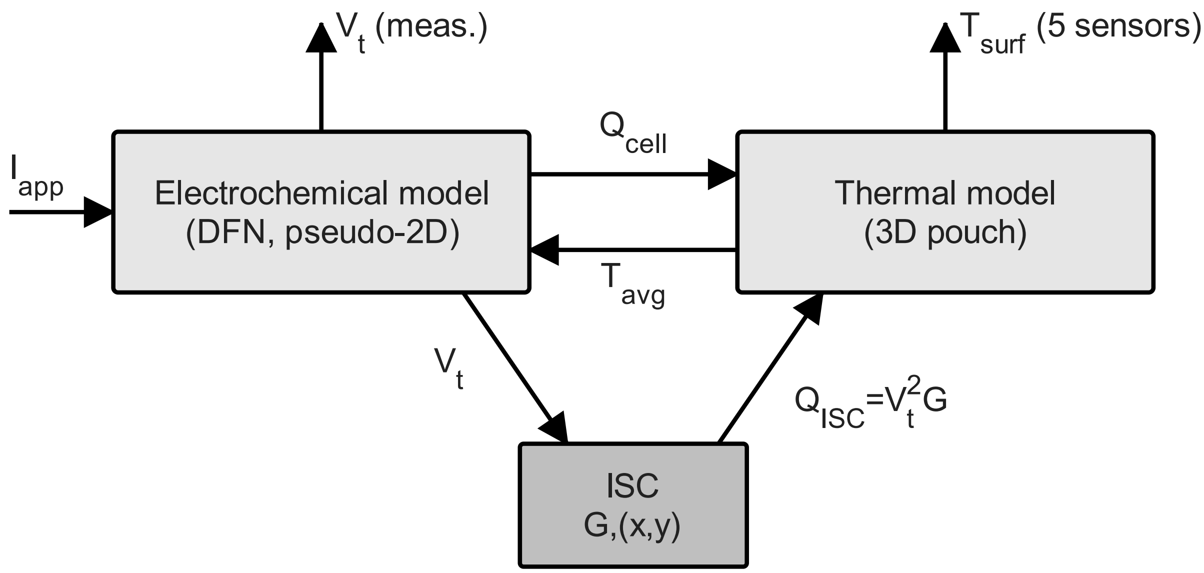

Figure 1. Two-way electro-thermal coupling in the plant. The electrochemical model and the thermal model exchange heat generation and temperature; the internal short circuit taps the local voltage and injects ohmic heat at its location.

Uhlmann, 2004). Joint estimation is preferred to a decoupled cascade because it preserves the cross-covariance between the conductance, the thermal field and the location: the short power $Q_{\mathrm{ISC}} = V_t^2 G$ links severity to the thermal measurements, so the temperature sensors help constrain G, not only the voltage. The fault parameters are initialized at a deliberately wrong "no-fault, centered" prior with large variance, so that the filter is free to move to the true values on the first informative measurement, and are clamped to physical bounds after each update. The filter settings, the noise covariances and the gate and detection thresholds are collected in Table 1.

4.2. Identifiability and Observability Considerations

The three fault parameters do not enter the measurements in the same way, and this asymmetry, rather than any property of the filter, dictates the structure of the estimator. The conductance appears explicitly in the output map: differentiating Eq. (1) gives $\partial V_t/\partial G = -R_0 V_t/(1 + R_0 G)$, which is finite and non-vanishing over the whole severity range considered, so G is structurally identifiable from the voltage channel alone as soon as its effect exceeds the voltage noise. This is why the conductance is the first fault parameter to converge in every run.

The position, by contrast, is absent from the electrical equations and reaches the measurements only through the thermal path. Up to the fixed linear transfer from the nodes to the sensor locations, the sensitivity of the measured temperatures to the fault position is

$$\frac{\partial \mathbf{T}_{\mathrm{sens}}}{\partial (x,y)} \propto Q_{\mathrm{ISC}} \frac{\partial \mathbf{w}(x,y)}{\partial (x,y)}, \qquad Q_{\mathrm{ISC}} = V_t^2 G. \quad (5)$$

Two consequences follow. First, the position is identifiable only to the resolution with which five sensors sample the kernel $\mathbf{w}$: two locations that produce the same five nodal temperatures cannot be told apart, so the layout, not the estimator, sets the localization floor — the quincunx is used precisely because it breaks the symmetry that a purely central or purely peripheral arrangement would leave. Second, the sensitivity in Eq. (5) scales with the short power and therefore vanishes with G, so G and (x, y) are only weakly *jointly* identifiable at low severity, where a weak nearby source and a stronger distant one produce nearly the same sensor readings. The gate described next is the practical consequence of this coupling, and the loss of localization at $R_{\mathrm{ISC}} = 100\ \Omega$ reported in Section 5 is the severity at which the right-hand side of Eq. (5) falls below the temperature noise. A formal observability analysis of the augmented system and a systematic study of sensor placement are left to future work.

4.3. Location-Observability Gate

A short of the severities considered here perturbs the terminal voltage from the first samples, so the conductance becomes observable early; the fault becomes *localizable* only once it has produced a measurable spatial temperature contrast, which occurs much later and, for weak faults, not at all. Updating the position before then couples the still-unsettled severity estimate into the location through Q_{ISC} and drives spurious motion. The location update is therefore gated: the position state is held until the measured spatial spread across the sensors exceeds a fixed threshold for a number of consecutive samples, after which the gate latches open. Gating on the *measurement* rather than the covariance avoids the self-

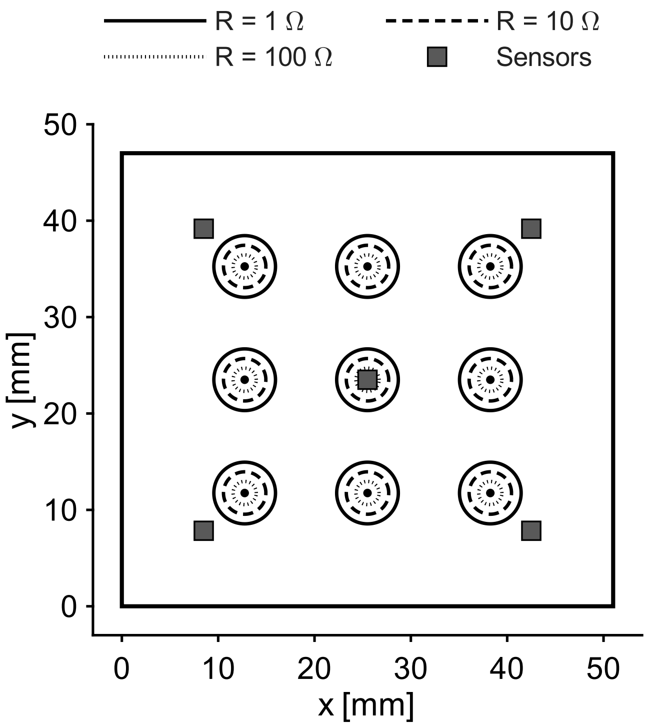

Figure 2. Design of experiments on the pouch cell: 3×3 grid of ISC locations, three severities per site ($R_{\mathrm{ISC}} = 1, 10, 100\ \Omega$, nested rings), and the five surface temperature sensors (squares).

locking behavior of covariance-based gates, and the held covariance is kept consistent by decoupling the position block while it is frozen.

4.4. Detection by Covariance Convergence

Rather than declaring detection when a state crosses an arbitrary threshold, the detection instant is defined as the time at which the filter *uncertainty* converges to a stable value, i.e. when the estimate stops improving and the filter has extracted the information the data contain. Operationally, detection is the first sample at which the relevant standard deviation has fallen below a fraction of its prior (so the filter has demonstrably learned something) and its relative variation over a trailing window is below a small tolerance (so it has flattened). This yields a confidence-based, parameter-agnostic detection time computed directly from the covariance the filter already maintains.

The criterion is heuristic in form but admits a clear informational reading. For a converging filter the posterior variance of a parameter is a non-increasing function of the information accumulated from the measurements, so a variance that has both fallen well below its prior and stopped changing indicates that further samples carry negligible additional information about that parameter. Detection declared on this event is therefore a statement that the available data have been exhausted, not that a signal has crossed a level, which makes the criterion independent of the fault magnitude and free of any tuned alarm threshold. Its limitation is the converse and is stated here explicitly: under model mismatch a filter can become confident about a biased estimate, so the detection time must be read together with the severity error, as is done in Section 5.

Table 1. Observer model, filter tuning and diagnostic thresholds used for all 27 runs. Standard deviations are given rather than variances; L and W are the in-plane cell dimensions.

Setting	Value
Observer model	
ECM order (RC pairs)	3
Cell footprint $L \times W \times H$	$51 \times 47 \times 6.4$ mm
LPTN grid $N_x \times N_y$	11×11 (121 nodes)
Augmented state dimension	128
In-plane conductivity	21.8 $\mathrm{W\,m^{-1}K^{-1}}$
Convection coefficient h	35 $\mathrm{W\,m^{-2}K^{-1}}$
Heat-kernel spread σ_k	5 mm
Sampling interval Δt	5 s
LUT temperature clamp	[278.15, 318.15] K
UKF sigma points	
Spread α	0.6
Prior weight β	2
Secondary scaling κ	0
Measurement noise $\mathbf{R}$ (std)	
Voltage σ_V	10 mV
Surface temperature σ_T	0.10 K
Process noise $\mathbf{Q}$ (std, per sample)	
SOC	10^{-5}
Relaxation voltages	10^{-4} V
Nodal temperatures	0.05 K
Conductance G	2×10^{-3} S
Position x, y	$L/200,\ W/200$
Initial estimate and prior $\mathbf{P}_0$ (std)	
G_0 (deliberate no-fault prior)	10^{-6} S
(x_0, y_0)	cell center
SOC / V_{RC} / $\mathbf{T}$	0.02 / 1 mV / 0.5 K
G	0.5 S
x, y	$L/4,\ W/4$
Post-update clamp on G	$G \geq 10^{-6}$ S
Validity window and gate	
SOC floor for the G update	0.30
Voltage-knee trim V_{knee}	3.4 V
Gate threshold on sensor spread	0.5 K
Gate debounce	8 samples (40 s)
Covariance-convergence detection	
Drop below prior std	factor 0.5
Trailing window	10 samples
Relative flatness tolerance	5%

5. RESULTS AND DISCUSSION

The observer is run online on each of the 27 DoE scenarios. Severity is reported as the resistance $R_{\mathrm{ISC}} = 1/G$; because R_{ISC} is a nonlinear function of the estimated conductance, its uncertainty is propagated by the delta method, $\mathrm{var}(R_{\mathrm{ISC}}) \approx \mathrm{var}(G)/G^4$. Estimation quality is summarized

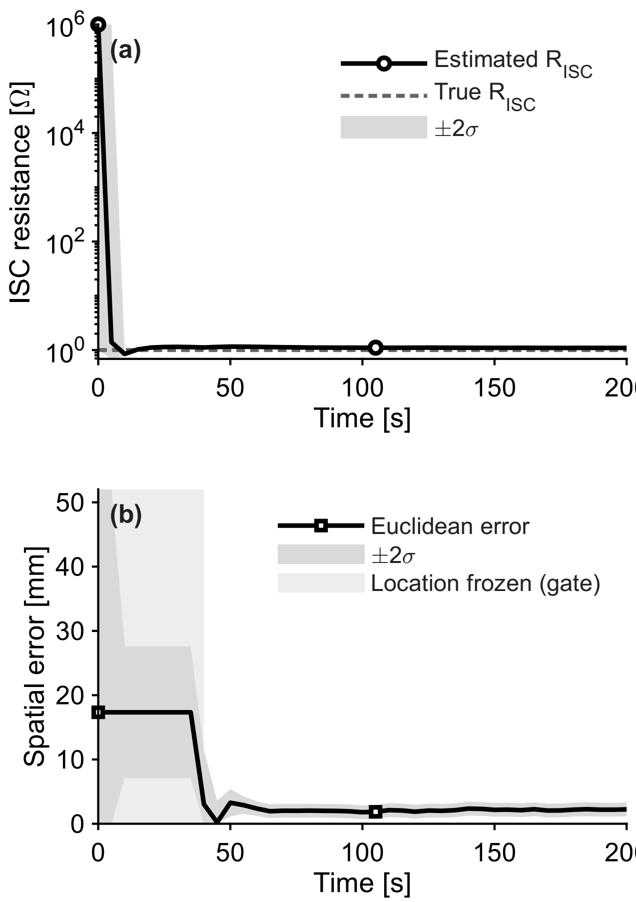

Figure 3. Representative run: (a) estimated ISC resistance R_{ISC} with $\pm 2\sigma$ band against the true value; (b) Euclidean localization error, with the gate-frozen interval shaded.

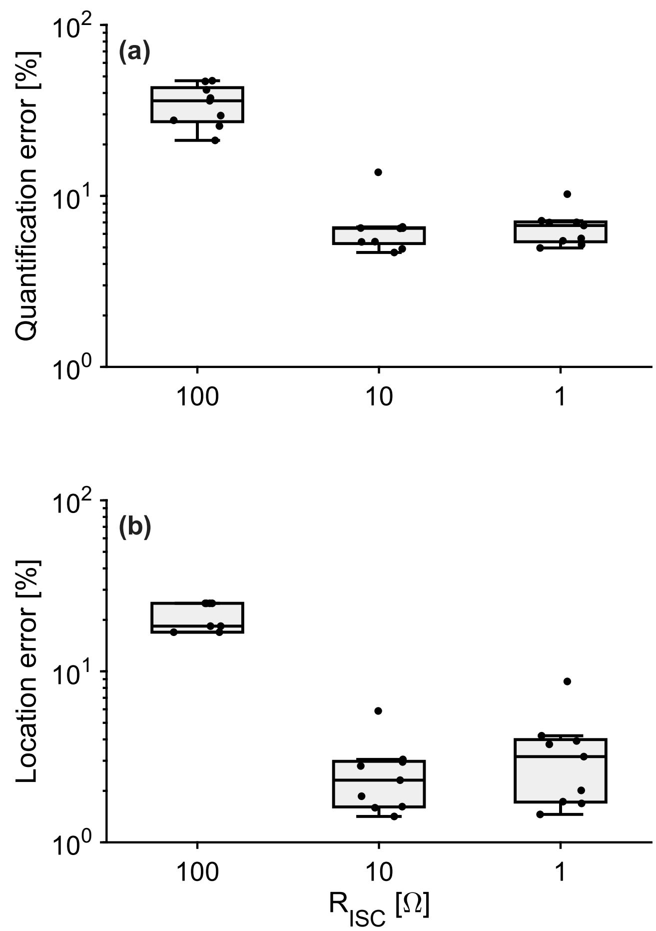

Figure 4. Distribution over the nine locations of (a) quantification error and (b) localization error (covariance-weighted NRMSE), versus short resistance R_{ISC}.

by a covariance-weighted normalized RMSE (so confident samples count more), evaluated over the analysis window, for both severity (normalized by the true resistance) and location (normalized by the cell diagonal). The 27 runs are executed in parallel and the prediction and covariance histories are stored for post-processing.

5.1. Representative Run

Figure 3 shows a representative strong-short case. The estimated resistance converges to the true value within the $\pm 2\sigma$ band, and the localization error decays to the millimeter level once the gate opens; the shaded interval marks the gated phase before the thermal contrast is informative. The covariance band tightens monotonically, which is what the convergence-based detection criterion exploits.

5.2. Severity Dependence

Figures 4 and 5 summarize performance across all nine locations at each severity. For $R_{\mathrm{ISC}} = 1$ and $10\ \Omega$ the observer performs well: the severity error is about 6–8$\%$ and the localization error about 2 mm (a few percent of the cell diagonal), with detection in roughly 110 s. Quantification and localization down to $R_{\mathrm{ISC}} = 10\ \Omega$ are therefore reliable.

At $R_{\mathrm{ISC}} = 100\ \Omega$ the behavior changes qualitatively and marks the detectability floor of the layout. The parasitic current is now a negligible fraction of the operating current, so the resistance is recoverable only to order of magnitude, with a severity error of tens of percent. More importantly, the deposited power is too small to raise a spatial thermal contrast above the gate threshold within the window, so the position is never updated and localization is not achieved; the apparent location error at this severity reflects the geometry of the held prior rather than estimator performance, and should be read as "not localized". This boundary is a property of the sensing arrangement, not of the estimator — it is the point at which the sensitivity of Eq. (5) drops below the temperature noise — and it quantifies how weak a short the present five-sensor layout can resolve.

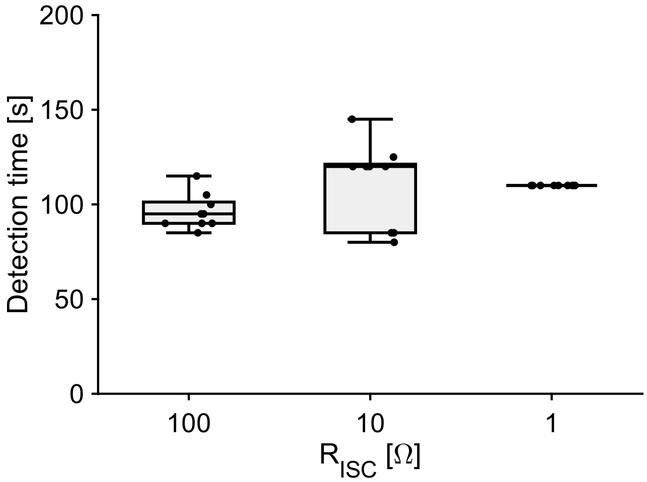

Figure 5. Distribution over the nine locations of the covariance-convergence detection time versus short resistance R_{ISC}.

5.3. Discussion

The results delineate a clear operating envelope: the single joint UKF detects, quantifies and localizes sub-critical internal shorts reliably for $R_{\mathrm{ISC}} \leq 10\ \Omega$, and degrades gracefully and interpretably at $R_{\mathrm{ISC}} = 100\ \Omega$, where severity becomes order-of-magnitude only and localization is limited by sensor thermal contrast rather than by the filter.

A residual few-percent bias on severity persists even for strong shorts; it originates from the mismatch between the reduced ECM used in the observer and the high-fidelity plant, and is consistent across locations, so it could be reduced by refining the ECM or by augmenting the state with a voltage-bias term. Because detection is defined on the covariance, the reported detection time reflects when the filter becomes confident; for very weak shorts the filter can converge confidently to a biased severity, which is why detectability is best discussed jointly with the severity-error and localization results.

The division of labor between the two sensing channels also deserves comment, since it is what justifies the added complexity of the electro-thermal formulation. The voltage channel is sufficient for detection and, at moderate and strong severities, for quantification; the temperature array is what makes localization possible at all, since the position does not appear in the electrical equations, and it additionally tightens the conductance estimate through the cross-covariance retained by the joint filter. A purely electrical observer would return severity without position and would lose the physical redundancy that keeps the severity estimate anchored when the ECM is imperfect.

Several limitations should be stated explicitly, and they bound the claims made above. First, the evaluation is entirely simulation-based. The plant is structurally different from the observer model, so the study is not a self-consistency check, but it cannot reproduce manufacturing variability, aging, sensor drift or contact-resistance effects, and experimental confirmation on cells with implanted shorts remains necessary. Second, the DoE varies severity and position while holding the operating condition fixed, so robustness across state-of-charge windows, current profiles and ambient temperatures is not established; the gate threshold in particular is expected to require rescaling with the ambient convective condition. Third, no quantitative benchmark against alternative observer-based ISC schemes is reported: the comparison offered in the Introduction is qualitative, and a fair numerical comparison would require re-implementing those schemes on the same plant. Fourth, the relative contribution of the two sensing modalities is argued above but not isolated by an ablation. Fifth, the DoE contains only faulted cases, so false-positive and false-negative rates over a population of healthy cells — the metrics that would ultimately govern deployment in a battery management system, where a false alarm is costly and a missed detection is unsafe — are not estimated. These points define the scope of an extended study.

6. CONCLUSION

A model-based observer for the online detection, quantification and localization of internal short circuits in lithium-ion pouch cells was presented. A compact coupled ECM–LPTN model represents the short as a conductance and a planar heat-source location, and a single joint unscented Kalman filter estimates these fault parameters together with the cell state from current, voltage and five surface temperatures. A measurement-based location-observability gate and a covariance-convergence detection criterion complete the scheme. Evaluated on a 27-case design of experiments produced by a high-fidelity electrochemical–thermal plant, the observer quantifies severity to within about 7% and localizes to about 2 mm for shorts of $R_{\mathrm{ISC}} \leq 10\ \Omega$, detecting in roughly 110 s, and identifies the detectability floor of the five-sensor layout at $R_{\mathrm{ISC}} = 100\ \Omega$. Future work will refine the observer ECM to reduce the residual severity bias, study sensor placement and count to lower the localization floor, quantify robustness across operating conditions and false-alarm rates on healthy cells, and validate the observer experimentally on cells with implanted shorts.

REFERENCES

Bernardi, D., Pawlikowski, E., & Newman, J. (1985). A general energy balance for battery systems. *Journal of the electrochemical society*, *132*(1), 5–12.

Besançon, G. (2000). Remarks on nonlinear adaptive observer design. *Systems & Control Letters*, *41*(4), 271–280.

Bizeray, A. M., Zhao, S., Duncan, S. R., & Howey, D. A. (2015). Lithium-ion battery thermal-electrochemical model-based state estimation using orthogonal collocation and a modified extended kalman filter. *Journal of Power Sources*, *296*, 400–412.

Doyle, M., Fuller, T. F., & Newman, J. (1993). Modeling of galvanostatic charge and discharge of the lithium/polymer/insertion cell. *Journal of the Electrochemical society*, *140*(6), 1526–1533.

Feng, X., Ouyang, M., Liu, X., Lu, L., Xia, Y., & He, X. (2018). Thermal runaway mechanism of lithium ion battery for electric vehicles: A review. *Energy storage materials*, *10*, 246–267.

Feng, X., Sun, J., Ouyang, M., Wang, F., He, X., Lu, L., & Peng, H. (2015). Characterization of penetration induced thermal runaway propagation process within a large format lithium ion battery module. *Journal of Power Sources*, *275*, 261–273.

Forgez, C., Do, D. V., Friedrich, G., Morcrette, M., & Delacourt, C. (2010). Thermal modeling of a cylindrical lifepo4/graphite lithium-ion battery. *Journal of power sources*, *195*(9), 2961–2968.

Hu, X., Li, S., & Peng, H. (2012). A comparative study of equivalent circuit models for li-ion batteries. *Journal of Power Sources*, *198*, 359–367.

Huang, L., Liu, L., Lu, L., Feng, X., Han, X., Li, W., ... others (2021). A review of the internal short circuit mechanism in lithium-ion batteries: Inducement, detection and prevention. *International Journal of Energy Research*, *45*(11), 15797–15831.

Julier, S. J., & Uhlmann, J. K. (2004). Unscented filtering and nonlinear estimation. *Proceedings of the IEEE*, *92*(3), 401–422.

Kang, Y., Duan, B., Zhou, Z., Shang, Y., & Zhang, C. (2019). A multi-fault diagnostic method based on an interleaved voltage measurement topology for series connected battery packs. *Journal of Power Sources*, *417*, 132–144.

Miao, Q., Xie, L., Cui, H., Liang, W., & Pecht, M. (2013). Remaining useful life prediction of lithium-ion battery with unscented particle filter technique. *Microelectronics Reliability*, *53*(6), 805–810.

Nascimento, R. G., Corbetta, M., Kulkarni, C. S., & Viana, F. A. C. (2021). Hybrid physics-informed neural networks for lithium-ion battery modeling and prognosis. *Journal of Power Sources*, *513*, 230526.

Rao, C. V., Rawlings, J. B., & Mayne, D. Q. (2003). Constrained state estimation for nonlinear discrete-time systems: stability and moving horizon approximations. *IEEE Transactions on Automatic Control*, *48*(2), 246–258.

Santhanagopalan, S., Ramadass, P., & Zhang, J. Z. (2009). Analysis of internal short-circuit in a lithium ion cell. *Journal of Power Sources*, *194*(1), 550–557.

Schwabacher, M., & Goebel, K. (2007). A survey of artificial intelligence for prognostics. In *Aaai fall symposium: artificial intelligence for prognostics* (pp. 108–115).

Seo, M., Goh, T., Park, M., Koo, G., & Kim, S. W. (2017). Detection of internal short circuit in lithium ion battery using model-based switching model method. *Energies*, *10*(1), 76.

Severson, K. A., Attia, P. M., Jin, N., Perkins, N., Jiang, B., Yang, Z., ... Braatz, R. D. (2019). Data-driven prediction of battery cycle life before capacity degradation. *Nature Energy*, *4*(5), 383–391.

Sulzer, V., Marquis, S. G., Timms, R., Robinson, M., & Chapman, S. J. (2021). Python battery mathematical modelling (pybamm). *Journal of Open Research Software*, *9*(1).

Wang, Q., Ping, P., Zhao, X., Chu, G., Sun, J., & Chen, C. (2012). Thermal runaway caused fire and explosion of lithium ion battery. *Journal of power sources*, *208*, 210–224.

BIOGRAPHIES

Lorenzo BRANCATO earned his bachelor's degree in mechanical engineering from the Politecnico di Milano in 2020. He then pursued a Master's degree in Mechatronic Engineering at the same institution, completing his studies in 2022. He obtained his Ph.D. in Mechanical Engineering from the Politecnico di Milano in 2026. His research focuses on developing advanced diagnostic and prognostic approaches for complex dynamic systems subject to degradation and faults. This involves high-fidelity multiphysics modeling and simulation, advanced model-based filtering methods, and advanced data-driven machine learning methods.

Yiqi JIA holds a Bachelor's degree in Automotive Engineering from Wuhan University of Technology, Wuhan, China (2017), and a Master's degree in Automotive Engineering from the University of Bath, Bath, UK (2018). After gaining valuable experience as a vehicle engineer at Ford Motor Company for almost three years, she commenced her Ph.D. in Mechanical Engineering at Politecnico di Milano in November 2021. She successfully completed her studies and was awarded her degree in June 2025. Her research is primarily focused on the diagnosis and prognosis of lithium-ion batteries. This includes battery modeling, simulation, data-based and model-based estimation methods for optimal battery management.

Danyang Wang holds a Bachelor's degree in Vehicle Engineering from Hefei University of Technology, China (2021), and a Master's degree in Vehicle Engineering from the Beijing Institute of Technology, Beijing, China (2025). He started his Ph.D. in Mechanical Engineering at Politecnico di Milano in November 2025. His research is primarily focused on the diagnosis and prognosis of lithium-ion batteries, structural batteries and, more broadly, on mechanical/structural-related behaviors.

Marco GIGLIO is Full Professor at the Department of Mechanical Engineering, Politecnico di Milano. His main research fields are: (i) Structural integrity evaluation of complex platforms through Structural Health Monitoring methodologies; (ii) Vulnerability assessment of ballistic impact damage on components and structures, in mechanical and aeronautical fields; (iii) Calibration of constitutive laws for metallic materials; (iv) Expected fatigue life and crack propagation behavior on aircraft structures and components; (v) Fatigue design with defects. He has been the coordinator of several European projects: HECTOR, Helicopter Fuselage Crack Monitoring and prognosis through on-board sensor, 2009-2011, ASTYANAX (Aircraft fuselage crack Monitoring System and Prognosis through eXpert on-board sensor networks), 2012-2015, and SAMAS (SHM application to Remotely Piloted Aircraft Systems), 2018-2020. He has been the project leader of the Italian Ministry of Defense project in the National Plan of Military Research, SUMO (Development of a predictive model for the ballistic impact), 2011-2012 and, SUMO 2 (Development of an analytical, numerical and experimental methodology for design of ballistic multilayer protections), 2017-2019. He has published more than 210 papers, h-index 27 (source Scopus) in referred international journals and congresses.

Francesco CADINI (MSc in Nuclear Engineering, Politecnico di Milano, 2000; MSc in Aerospace Engineering, UCLA, 2003; PhD in Nuclear Engineering, Politecnico di Milano, 2006) is Associate Professor at the Department of Mechanical Engineering, Politecnico di Milano. He has more than 20 years of experience in the assessment of the safety and integrity of complex engineering systems, entailing (i) artificial intelligence (machine learning)-based approaches for classification and regression, (ii) development and application of advanced Monte Carlo algorithms for reliability analysis (failure probability estimation), (iii) diagnosis and prognosis (HUMS) of dynamic, complex systems subject to degradation, (iv) uncertainty and sensitivity analyses, (v) structural reliability analyses.